

The Void Galaxy Survey: photometry, structure and identity of void galaxies

B. Beygu,^{1,6*} R.F. Peletier,¹ J. M. van der Hulst,¹ T. H. Jarrett,² K. Kreckel,³
R. van de Weygaert,¹ J. H. van Gorkom,⁴ M. A. Aragon-Calvo⁵

¹*Kapteyn Astronomical Institute, University of Groningen, PO Box 800, 9700 AV Groningen, the Netherlands*

²*Astronomy Department, University of Cape Town, Rondebosch 7700, Cape Town, South Africa*

³*Max Planck Institute for Astronomy, Königstuhl 17, 69117 Heidelberg, Germany*

⁴*Department of Astronomy, Columbia University, Mail Code 5246, 550 West 120th Street, New York, NY 10027, USA*

⁵*University of California, 900 University Avenue, Riverside, CA 92521, USA*

⁶*Physics and Centre for Space Research, North-West University, Potchefstroom, South Africa*

Last updated 2016 January 7

ABSTRACT

We analyze photometry from deep B-band images of 59 void galaxies in the Void Galaxy Survey (VGS), together with their near-infrared $3.6\mu\text{m}$ and $4.5\mu\text{m}$ Spitzer photometry. The VGS galaxies constitute a sample of void galaxies that were selected by a geometric-topological procedure from the SDSS DR7 data release, and which populate the deep interior of voids. Our void galaxies span a range of absolute B-magnitude from $M_B = -15.5$ to $M_B = -20$, while at the $3.6\mu\text{m}$ band their magnitudes range from $M_{3.6} = -18$ to $M_{3.6} = -24$. Their B-[3.6] colour and structural parameters indicate these are star forming galaxies. A good reflection of the old stellar population, the near-infrared band photometry also provide a robust estimate of the stellar mass, which for the VGS galaxies we confirm to be smaller than $3 \times 10^{10} M_\odot$. In terms of the structural parameters and morphology, our findings align with other studies in that our VGS galaxy sample consists mostly of small late-type galaxies. Most of them are similar to Sd-Sm galaxies, although a few are irregularly shaped galaxies. The sample even includes two early-type galaxies, one of which is an AGN. Their Sérsic indices are nearly all smaller than $n = 2$ in both bands and they also have small half-light radii. In all, we conclude that the principal impact of the void environment on the galaxies populating them mostly concerns their low stellar mass and small size.

Key words: galaxies: evolution — galaxies: formation — galaxies: structure — large-scale structure of universe

1 INTRODUCTION

Voids are prominent features of the cosmic web (van de Weygaert & Platen 2011). Formed from primordial underdensities they now occupy a major fraction of the volume of the universe, surrounded by denser filaments, walls and sheets. They are the most underdense regions where galaxy evolution will have progressed slowly, without the dominant and complex influence of the environment. Voids therefore are extremely well suited for assessing the role of the environment in galaxy evolution, as here the galaxies are expected not to be affected by the complex processes that modify galaxies in high density environments. The void environment covers the lowest density environments found in the universe, though some voids do approach similar (and still

low) densities as found in tenuous filaments and walls (Cautun et al. 2014).

In order to get a good picture of galaxies in voids the Void Galaxy Survey (VGS) was designed, a multiwavelength study of 59 galaxies in geometrically defined voids (Stanonik et al. 2009; van de Weygaert et al. 2011; Kreckel et al. 2011a, 2012; Beygu et al. 2016). Previous papers based on the Void Galaxy Survey have focused on the HI properties of galaxies in voids (Kreckel et al. 2011a, 2012; Beygu et al. 2013) and on the star formation properties of void galaxies (Beygu et al. 2016). They found that voids contain a population of galaxies that are relatively HI rich of which many present evidence for ongoing gas accretion, interactions with small companions and filamentary alignments.

Even though based on a wide variety of selection methods, previous studies have lead to the general contention that void galaxies appear to be blue and low-luminosity galaxies

* E-mail: burcu.beygu@nwu.ac.za

with stellar masses lower than the average galaxy - typically in the order $3 \times 10^{10} M_{\odot}$ - and of a late morphological type, residing in a more youthful state of star formation and possessing larger and less distorted supplies of gas (Szomoru et al. 1996; Kuhn et al. 1997; Popescu et al. 1997; Karachentseva et al. 1999; Grogin & Geller 1999, 2000; Rojas et al. 2004, 2005; Croton et al. 2005; Goldberg et al. 2005; Hoyle et al. 2005; Tikhonov & Karachentsev 2006; Patiri et al. 2006a,b; Ceccarelli et al. 2006; Wegner & Grogin 2008; Kreckel et al. 2012; Beygu et al. 2016). Penny et al. (2015) recently reported to have found some galaxies with stellar masses $10^{10} M_{\odot} < M_{*} < 5 \times 10^{11} M_{\odot}$ that are located in voids, although the identification with underdense regions similar to those of our study is not clear.

The pristine environment of voids represents an ideal and pure setting for the study of environmental influences on galaxy formation and evolution. The clearest indication for the significance of environmental influences on galaxy properties is the tight relation between morphology and density (Oemler 1974; Dressler 1980; Dressler et al. 1985). The fraction of elliptical and lenticular galaxies rises steeply with increasing environmental density. This goes along with the opposite trend for late-type and irregular galaxies, down towards the lowest density regions. This can be understood by observing that the evolution of galaxies in high-density regions is strongly influenced by the complex interplay of a range of physical processes, mostly induced by the interaction of galaxies amongst themselves and the intergalactic medium. Processes such as quenching, ram pressure, strangulation and tidal stripping render galaxies gas poor, yielding reddish galaxies (Gunn & Gott 1972; Larson et al. 1980; Moore et al. 1996; Koopmann & Kenney 2004; Gabor et al. 2010; Peng et al. 2010; Wetzel et al. 2012). In more moderate and low density regions these processes cease to be effective, explaining the increasing fraction of late-type and gas-rich galaxies. An additional and related environmental influence that manifests itself in voids and that still needs to be understood is the finding that void galaxies appear bluer, a trend that continues down into the most rarefied void regions.

For the purpose of better understanding environmental influences on the evolution of galaxies, recent years saw a considerable increase of interest in the nature of void galaxies (Kreckel et al. 2011a, 2012; Hoyle et al. 2012; Beygu et al. 2013; Alpaslan et al. 2014; Moorman et al. 2014; Kreckel et al. 2015; Tavasoli et al. 2015; Penny et al. 2015; Moorman et al. 2015; Beygu et al. 2016). Amongst the issues relevant for our understanding of galaxy and structure formation, void galaxies have posed several interesting riddles and questions. Arguably the most prominent issue is that of the near absence of low-luminosity galaxies in voids, while standard LCDM cosmology expects voids to be teeming with dwarfs and low-surface-brightness galaxies (Peebles 2001). An interesting point of focus for void galaxy studies has therefore been the study of dwarf galaxies in nearby voids, such as in the Boötes, Lynx-Cancer, Hercules and Eridanus void (Grogin & Geller 2000; Cruzen et al. 2002; Petrov et al. 2005; Pustilnik et al. 2011, 2013). Kreckel et al. (2011b) made a detailed HI study of the dwarf KK246 in the Local Supercluster, one of the darkest galaxies known with an M/L = 89. Another recent example concerns the study by Karachentsev & Kaisina (2013), who looked for faint void galaxies,

not brighter than the Magellanic Clouds, in the Local Supercluster and immediate vicinity out to a distance of 40 Mpc. They found no less than 89 voids which do not appear to contain any galaxies brighter than $M_K < -18.4$. One of these voids is the Local Void.

Another issue of interest is whether we can observe the intricate filigree of substructure in voids, expected as the remaining debris of the merging of voids and filaments in the hierarchical formation process (van de Weygaert & van Kampen 1993; Sheth & van de Weygaert 2004; van de Weygaert & Platen 2011; Aragon-Calvo 2012). Evidence for such substructure, three interacting galaxies embedded in a common HI envelope, has been reported by Beygu et al. (2013), who hypothesised it to be an assembly of a filament in a void.

Of key importance towards deciphering the nature and evolutionary history of void galaxies are their structural properties. Most of the previous observational studies of void galaxies were based on an analysis of photometric data from existing all sky surveys, such as the Sloan Digital Sky Survey and the Center for Astrophysics Redshift Survey (Hoyle & Vogeley 2002; Rojas et al. 2004, 2005; Patiri et al. 2006b; Hoyle et al. 2012; Tavasoli et al. 2015; Alpaslan et al. 2015; Penny et al. 2015). Lately, also within the context of the Galaxy Mass and Assembly Survey (GAMA, Driver et al. (2011)) considerable attention has been devoted to voids and void galaxies (Alpaslan et al. 2014, 2015; Penny et al. 2015). Using catalogues of large-scale structure including voids, group and pair membership from the GAMA survey, Alpaslan et al. (2015) examined the galaxy properties and found that the stellar mass is the dominant factor in shaping the galaxy properties. Such studies are limited in depth or resolution because of the magnitude limits of the surveys. The present study of the galaxies in the Void Galaxy Survey focusses on the analysis of deeper photometric data that we obtained for the VGS galaxies, to assess their colour, stellar mass, galaxy concentration, morphology and specific star formation. We use deep B-band and $3.6\mu\text{m}$ near-infrared imaging to investigate the structural characteristics and morphologies of galaxies in the Void Galaxy Survey (VGS, see section 2). The analysis involves the determination of the total luminosity, characteristic scale r_e and the surface brightness μ_e of the galaxies, along with the concentration of the stellar population, quantified by the Sersic index n . The inferred measurements are compared to literature values of structural parameters for a wide range of different galaxies. Amongst these are late-type disk galaxies, dEs as well as giant early-type galaxies.

By using photometry in three bands, two near-infrared and one optical, our photometric study yields important insights into the morphology and stellar populations of the VGS galaxies. The deep B-band images trace both the younger and older population. A unique aspect of our study is the inclusion of the Spitzer $3.6\mu\text{m}$ and $4.5\mu\text{m}$ imaging data. In particular the $3.6\mu\text{m}$ band data represents a major asset for our understanding of the stellar population of these galaxies, given the insensitivity of the $3.6\mu\text{m}$ band images to dust extinction and the fact that they provide a good reflection of the old stellar population in these galaxies (see e.g. Peletier et al. (2012) and Meidt et al. (2014) for a discussion). This also means that the $3.6\mu\text{m}$ flux, together with the [3.6]- [4.5] colour provide us with a robust estimate of

the stellar mass of a galaxy, since the old stellar population constitutes its major share. In addition, by combining information on the young and older stellar populations, the B-[3.6] colour provides us with a good indicator of the composition of the stellar population.

In addition, we seek to extract information on the star formation and evolution of void galaxies. From the colour comparison of B-band photometry with the Spitzer 3.6 μ m band photometry of the void galaxies, we assess their star formation histories. This information is combined with the results obtained from near-UV imaging to infer colours and the specific star formation rates SFR_{NUV}/M_* (see [Beygu et al. \(2016\)](#)).

The paper is organized as follows: In section 2 we describe the VGS sample and the results found so far. Section 3 contains a description of the observations and the data analysis. In section 4 we subsequently present the morphology of the void galaxies, and attempt to relate this to their underdense void environment. In the same section, we present and briefly discuss the structural parameters of these galaxies. The star formation properties and evolution of the stellar population form the subject of section 5. Finally, in section 6 and section 7 we shortly discuss and summarize our findings.

2 THE VGS SAMPLE

The Void Galaxy Survey (VGS) ([van de Weygaert et al. 2011](#); [Kreckel et al. 2011a, 2012](#); [Beygu et al. 2016](#)) is a systematic multiwavelength survey of 59 void galaxies, aiming to probe the colour, morphology, star formation and gas content of the void galaxies. For this we observed the VGS galaxies at radio wavelengths, in the 21-cm line, in H α and in the optical B-band. In addition, we acquired GALEX near-UV data on the VGS galaxies, as well as Spitzer 3.6 μ m imaging. For some we obtained CO(1-0) observations, which will form the starting point for a study of the relation between their star formation activity and their molecular and atomic gas content.

Our VGS galaxy sample has been selected from the Sloan Digital Sky Survey Data Release 7 (SDSS DR7). We exclusively used geometric and topological techniques for delineating voids in the galaxy distribution and identifying galaxies populating the central interior of these voids ([Schaap & van de Weygaert 2000](#); [Platen et al. 2007](#); [Aragón-Calvo et al. 2010b](#); [Kreckel et al. 2011a](#)). The typical size of voids in our sample is on the order of 5 to 10 Mpc. The resulting sample of void galaxies is unbiased and largely independent of intrinsic galaxy properties (except for the selection criteria defined by the SDSS). The importance of this is that it may be used towards obtaining an optimally representative census of the properties of galaxies that are located in the most diluted regions of the Universe. The detection of the void galaxies is limited to the spectroscopic flux limit of 17.7 mag in the r-filter of the SDSS. The VGS galaxies have redshifts in the range $0.02 < z < 0.03$, while they have an absolute magnitude in the range of $-20.4 < M_r < -16.1$, and colours in between $0.6 < g - r < 0.87$ ([Kreckel et al. 2011a, 2012](#)).

So far we have completed the study of the HI ([Kreckel et al. 2012](#)) and star formation properties ([Beygu et al. 2016](#)) of the VGS sample. We detected 41 of them in HI, with

total masses ranging from 1.7×10^8 to $5.5 \times 10^9 M_\odot$. We found that many have extended HI disks. Often these are morphologically and kinematically disturbed, showing signs of ongoing gas accretion. In addition, we found 18 HI-rich neighbouring galaxies within a radial distance of 100 km s^{-1} from the targeted galaxy. However, we have not been able to establish the presence of any significant number of HI-rich low-luminosity galaxies that would fill the void ([Kreckel et al. 2012](#)). As such, we found no indication for the existence of a large population of dwarf galaxies, whose presence would be expected according to theoretical expectations ([Peebles 2001](#)).

What we did find are several interesting and at first unexpected peculiar void galaxies. One of these is a polar ring galaxy, VGS_12, located in a tenuous wall between two voids ([Stanonik et al. 2009](#)). We also found a configuration of three void galaxies, VGS_31, aligned along what appears to be a tenuous filament along a void ([Beygu et al. 2013](#); [Rieder et al. 2013](#)). We compared their H α star formation rates per stellar and per HI mass with those for galaxies in moderate underdensity regions of the cosmic web and found only a marginal increase in star formation rates ([Beygu et al. 2016](#)). Their optical emission line and infrared colour properties show that the VGS galaxies are star forming galaxies with the exception of one passive galaxy.

3 OBSERVATIONS

B-band imaging has been obtained with the Wide Field Camera (WFC) at the 2.5m Isaac Newton Telescope (INT) at the Observatorio del Roque de los Muchachos at La Palma using the Johnson-Cousins B-filter between March 2010 and March 2012. Total exposure times were 2400 seconds, spread over 4 exposures for the purpose of dithering and facilitating cosmic ray detection. The average seeing was 1.4 arcsecond and the pixel scale is 0.33 arcsec/pixels. Flat-field exposures were taken at twilight at the beginning and/or end of each night.

The near-infrared data have been obtained from the Spitzer 3.6 μ m and 4.5 μ m, observed for the program 80069. We used the Spitzer-IRAC [3.6] Level 2 (post-BCD) data, which have been calibrated by the Spitzer-IRAC pipeline. The pixel scale is 0.6 arcsec/pixels. To understand the IRAC 3.6 micron PSF we note that the original pixel size was 1.2", and that the data were severely undersampled (the diffraction limit of Spitzer at 3.6 micron is only 1.05" (FWHM)), giving an effective FWHM_{PSF} of about 1.6". Here we do not use any data inside 2.4" for fitting the surface brightness distributions.

3.1 Data reduction

The INT data have been reduced using the standard IRAF¹ procedures for CCD imaging. All the optical images were trimmed and overscanned, followed by bias subtraction and flat fielding. After that all images from each filter were aligned and median combined. Photometric calibrations have been done by calibrating each science frame using 3

¹ <http://iraf.noao.edu/>

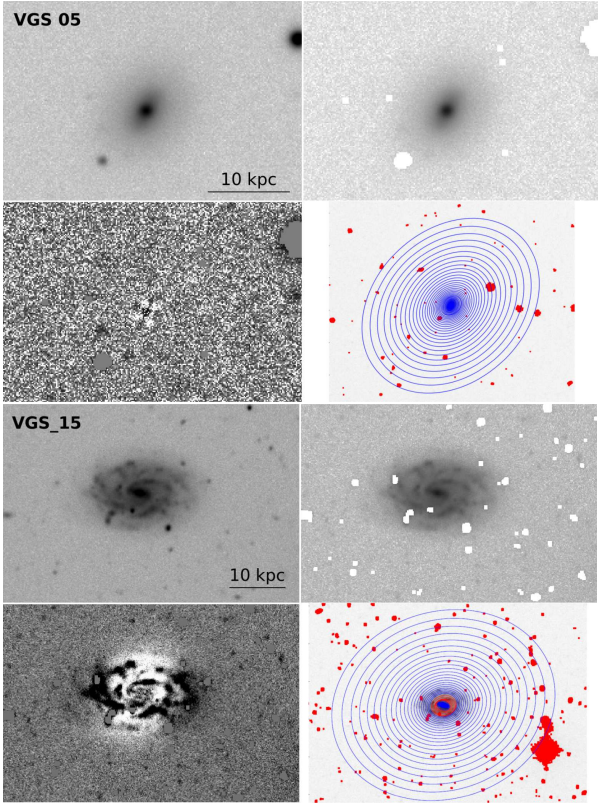


Figure 1. Raw, cleaned and model-subtracted images and resulting ellipse fits for B-band created by ARCHANGEL (clockwise from left) for VGS_05 (top) and VGS_15 (bottom). (A colour version of this figure is available in the online journal.)

SDSS stars with $g < 17$. To do this, SDSS g band magnitudes were converted to the Johnson-Cousins B photometric system following the relation given in Fukugita et al. (1996):

$$g - r = 0.93 \times (B - V) - 0.06, \quad (1)$$

We converted our IRAC counts to magnitudes on the Vega magnitude system, using the fact that IRAC $3.6\mu\text{m}$ has a flux density of zero magnitude source of $F_\nu = 280.9$ Jy, and $4.5\mu\text{m}$ has $F_\nu = 179.7$ Jy, implying that 1 count/sec corresponds to 18.80 Mag in the [3.6] band, and 18.32 in the [4.5] (IRAC Instrument Handbook²).

After this, aperture photometry has been performed using the galaxy photometry package ARCHANGEL (Schombert 2007) for both B-band IRAC [3.6] and [4.5] band images. The Archangel photometry tool performs the following steps: i) cleaning, flattening and sky determination of the science frame. Foreground stars are masked during the cleaning procedure. The sky is determined using sky boxes placed in the frame avoiding stars and far away from other galaxies. An iterative mean and σ are calculated for each box. They are then averaged to find the value of the sky. ii) isophotal fitting where elliptical isophotes are used. Archangel allows that position angles and ellipticities can be kept frozen at all radii. In this work these parameters are freely determined. Any pixels above (or below) a multiple of

the RMS around the ellipse are masked along an isophote. These masked regions are later restored for aperture photometry. iii) conversion of the 2D information to 1D surface brightness profiles. iv) profile fitting.

Figure 1 shows raw, cleaned, model-subtracted and ellipse-fitted images of two galaxies (VGS_05 and VGS_15) as examples. An inner radial cutoff has been applied to account for the uncertainty caused by the seeing for the B-band images. Upper radial cutoffs are put where the background starts to dominate. In the case of Spitzer images, the inner cutoff is always constant and equals 2.4 arcseconds. In the B-band it is twice the FWHM of the seeing, after Franx et al. (1989) and Peletier et al. (1990). Following this, total magnitudes (m_{tot}) and effective radii were derived using curves of growth from the ellipse-fitting results for both wavelengths. Given it is not model dependent, this produces reliable results. For the Spitzer IRAC imaging errors on the total magnitudes are dominated by the sky background errors which are 0.1 mag. As for the B-band, errors on the total magnitudes are smaller than a combination of the errors on the zeropoint and the sky background, which is 0.2 mag.

The B-band magnitudes are corrected for galactic extinction using Schlegel et al. (1998). The effective surface brightness, μ_e , is defined as the surface brightness at the effective radius r_e (half-light radius) and is determined using curves of growth. It is defined as the radius at which the magnitude reaches:

$$m(r_e) = m_{\text{tot}} + 2.5 \times \log 2, \quad (2)$$

Surface brightness profiles have been fit to a one component Sérsic function (Graham & Driver 2005) that gives the Sérsic index n , such that

$$I(R) = I_e \exp \left\{ -b_n \left[\left(\frac{R}{R_e} \right)^{1/n} - 1 \right] \right\}, \quad (3)$$

where $n = 1$ is typically assumed to correspond to the exponential disk profile of disk galaxies, and $n = 4$ to the de Vaucouleurs profile of ellipticals. In Figure 2, Sérsic profile fitting for VGS_05 and VGS_15 is shown for the B-band.

Traditionally, late-type galaxies are described in terms of their disc scalelength, h , and central surface brightness, μ_0 . The disk and bulge are often fit separately as well. In our study, we are challenged by the relatively low resolution of the data (caused by seeing and sampling) compared to the size of the galaxies, so we only fit one Sérsic law, a technique which is often used for distant galaxies. We have also applied a pure disk profile using a bulge + disk fit with a zero-sized bulge according to Freeman (1970) and Kent (1985) as:

$$I(R) = I_0 \exp(-hR), \quad (4)$$

$$\mu(R) = \mu_0 + 1.082 \left(\frac{R}{h} \right), \quad (5)$$

We have converted our effective surface brightness, μ_e , to the mean effective surface brightness $\langle \mu \rangle_e$, assuming the Sérsic index $n = 1$, following the recipe in Graham & Driver (2005):

$$\langle \mu \rangle_e = \mu_e - 0.699 \quad (6)$$

² <http://irsa.ipac.caltech.edu/data/SPITZER/docs/irac/>

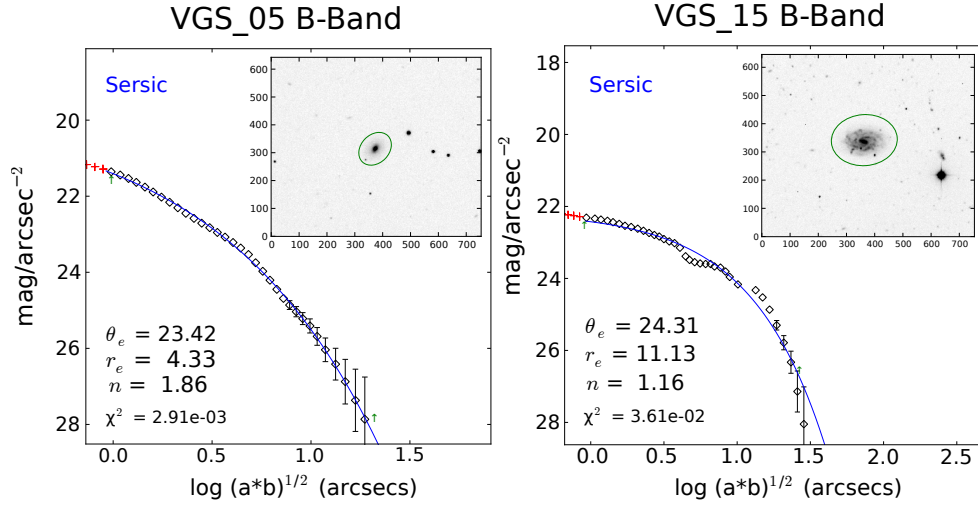


Figure 2. Final surface photometry profile for VGS_05 and VGS_15. Solid lines are the fit to a one-component Sérsic function. a and b are the major and the minor axis of the ellipse, respectively. Red crosses represent the inner cut-off regions. (A colour version of this figure is available in the online journal.)

Stellar masses are calculated using the $[3.6]-[4.5]$ colours via the empirical mass-to-light ratio given in Querejeta et al. 2014 as:

$$\log(M/L) = -0.339(\pm 0.057) \times ([3.6] - [4.5]) - 0.336(\pm 0.002) \quad (7)$$

for an assumed $M/L_{3.6\mu m} = 0.6 M_{\odot}/L_{\odot}$ for the old stellar population.

3.2 Consistency assessment of the data

To check the consistency of our measurements, we compare the various structural parameters with values found in the literature. The optical B-band total magnitude, effective radius and stellar mass estimates of the galaxies in our sample are compared with literature values obtained on the basis of SDSS data. We converted the SDSS g-band model magnitudes to the Johnson-Cousins B system and compared them to our B-band magnitudes in Figure 3 (top panel). The mean difference is ~ -0.02 with $\sigma \sim 0.2$ magnitude.

The effective radius is determined on the basis of a Sérsic fit. The stellar mass estimates are obtained from the MPA/JHU catalogue for SDSS DR7³. The comparison also involves the magnitudes from the near-infrared Spitzer $[3.6]$ band photometry, which is compared to WISE $[3.4]$ band (W1) magnitudes, and the stellar mass inferred from the $[3.6]$ band image.

We compared our $[3.6]$ band magnitudes to the 1σ isophotal magnitudes of W1 which are determined with profile-fitting photometry (Figure 3, bottom panel). The reduced chi-square, $(\chi^2)_{W1}$, of this isophotal fit gives a measure for an object to be classified either as a point source or a resolved source. If the $(\chi^2)_{W1} < 2$, then the object is considered as an unresolved source (point source), otherwise a resolved source (extended source). Due to their small

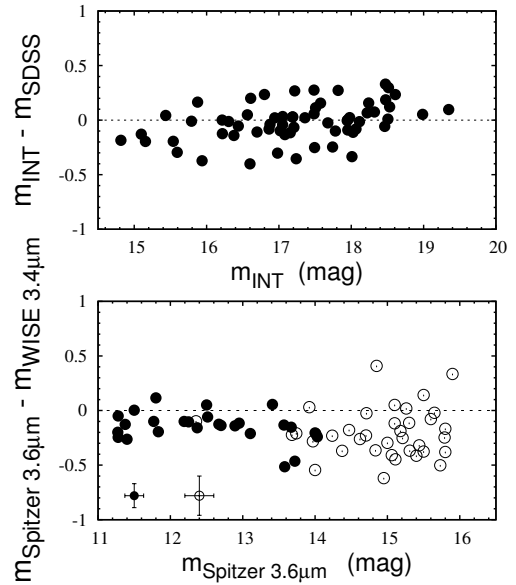


Figure 3. Top: INT B magnitudes compared to SDSS g-band model magnitudes converted to the Johnson-Cousins B system. Bottom: Spitzer $[3.6]$ band magnitudes compared to WISE $[3.4]$ band magnitudes. Open circles are defined as point source by the WISE pipeline, for which $\chi^2 < 2$ for the $3.4\mu m$ profile-fit photometry.

size, most of the unresolved VGS galaxies are not resolved by WISE and Spitzer. Some are heavily contaminated by the foreground stars, making it difficult to perform aperture photometry on these objects. In the bottom panel of Figure 3, we use the total magnitudes determined by isophotal and extrapolated fits for the objects resolved by WISE and magnitudes determined by isophotal fits for those that are unresolved. In this figure open circles represent VGS galaxies that are not resolved in W1 and the filled circles represent those that are resolved. There is a significant difference between the residuals of the resolved and the unresolved VGS

³ The MPA-JHU catalogue is publicly available and may be downloaded from <http://www.mpa-garching.mpg.de/SDSS/DR7/archive>.

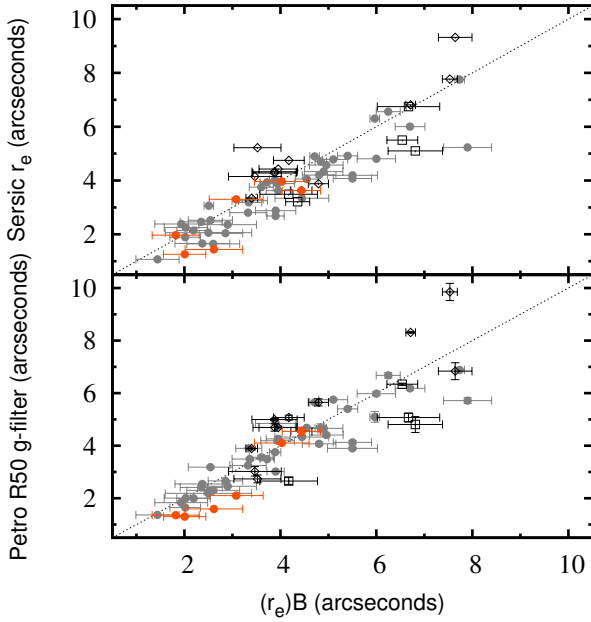


Figure 4. Comparison of $(r_e)_B$ to the Sérsic effective radius (top) and to the SDSS Petrosian half-radius R50 in g-filter (bottom). Galaxies with $\text{FWHM}_{\text{PSF}} < 2$ arcseconds are shown as grey and those with $\text{FWHM}_{\text{PSF}} \geq 2$ arcseconds are shown as orange. Open squares represent irregular galaxies and open diamonds represent edge-on galaxies. See main text for the definition of the classification for “irregular” and “edge-on”. The unity line is shown as dashed grey line. (A colour version of this figure is available in the online journal.)

galaxies. The difference is most likely caused by the fact that the WISE magnitudes are isophotal magnitudes; given the much higher S/N of the Spitzer data, we argue that our measurements are fine, with scatter < 0.3 mag.

In order to show the effects of the seeing, sky and the limited radial range on our photometric analysis we compare the effective radii in the B-band to those derived via Sérsic fits (Sérsic r_e) (Figure 4, top panel) and to the SDSS Petrosian half-radius R50 in the g-filter (R_{P50}) (Figure 4, bottom panel). Errors on the $(r_e)_B$ are due to the uncertainties in the accuracy of sky subtraction. The SDSS algorithm uses a modified version of the Petrosian system (Petrosian 1976) that measures galaxy fluxes within a circular aperture, whose radius (r_P) is defined by the shape of the azimuthally averaged light profile⁴. R_{P50} is defined as the radius containing 50% of the flux within a certain number of r_P .

In Figure 4, galaxies which have an irregular appearance are shown as open squares. Galaxies that have inclination $i > 70^\circ$ according to Kreckel et al. (2012) are classified as edge-on and are shown as open diamonds in Figure 4. Galaxies that have relatively poor seeing ($\text{FWHM}_{\text{PSF}} \geq 2$ arcseconds) compared to the rest of the sample are shown in orange dots. The difference between our effective radii and the effective radii determined in both other ways are larger for these galaxies. The mean of $(r_e)_B$ -to-Sérsic- r_e ratio

is ~ 1.1 and the mean of $(r_e)_B$ -to- R_{P50} ratio is ~ 1.04 (VGS galaxies that are neither edge-on, irregular or that have poor seeing, are shown as grey dots in Figure 4). We expect the agreement with the Sérsic half-light radii to be worse, since the method to determine them is much less stable than the method using apertures. Our $(r_e)_B$ estimates are in agreement with the Petrosian half-radius R50 and the Sérsic effective radius according to the relation shown in Graham & Driver (2005). In the analysis that follows, we will use the effective radius determined via the curve of growth, because it is independent of any assumed model and the effective surface brightness that corresponds to this r_e .

4 MORPHOLOGY AND STRUCTURE OF THE VGS GALAXIES

In this section, we will discuss the morphology and structural parameters of the VGS galaxies. By comparing magnitude, Sérsic index, effective radius and effective surface brightness of our sample to the same properties of other galaxies of different Hubble types, we seek to learn more about the identity of the void galaxies. In addition, we will discuss the properties of the galaxies, including their HI content and the relationship with the low density of their void environment.

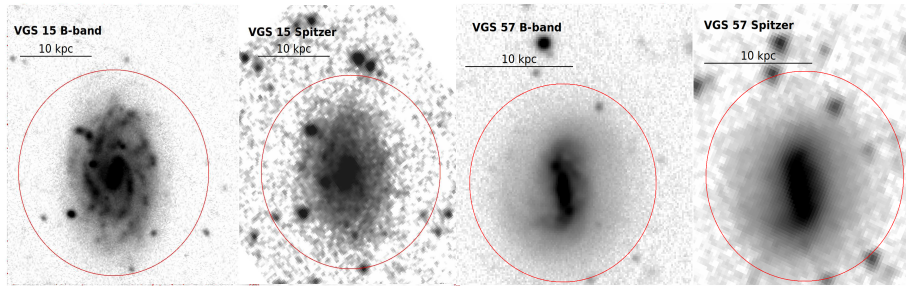
4.1 Morphology of the VGS galaxies

Morphological classification of galaxies involves rather specific issues, amongst others, high spatial resolution. An accurate classification requires a more elaborate analysis (see Buta 2013) than we are able to provide here. Therefore, instead of carrying out an absolute morphological classification, we seek to classify the morphology of the VGS galaxies in a general way by eye. We find that the VGS galaxy sample mainly consists of disk galaxies with an occasional bar and spiral structure. Amongst the VGS galaxies, a few objects are small and compact. Seven VGS galaxies have an irregular shape, twelve are edge-on systems ($i > 70^\circ$) while two objects are early-type galaxies. Five VGS galaxies — VGS_30, VGS_31, VGS_37, VGS_38 and VGS_54 — have nearby companions within 50 kpc. Some of these show signs of interactions, either in their optical or HI morphology, or in their kinematics (Kreckel et al. 2012; Beygu et al. 2013).

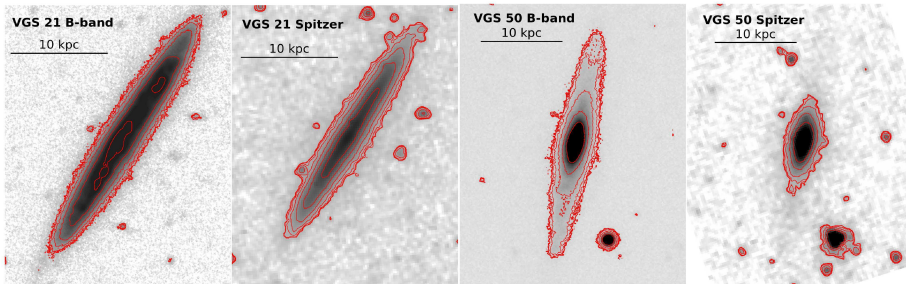
Eleven galaxies have neighbours and companions between 100 to 600 kpc, detected in HI. These galaxies do not have any HI connection with the main VGS galaxy and there is no spectral redshift information for them in the SDSS database. Also we do not have any information on their dynamical or stellar mass. Moreover, except for these companions our B-band images do not reveal a significant increase of dwarf galaxy resembling objects within 500 kpc distance from the identified void galaxy. Examples representing the different types of galaxies that constitute our sample are presented in Figure 5, in both B-band and [3.6] band. One of them, VGS_15, is a face-on spiral galaxy with tight spiral arms. These are clearly visible in the B-band, but not as pronounced in $3.6\mu\text{m}$. Its nuclear bulge is visible in both wavelengths. VGS_57 is a spiral galaxy with a bar that is bright in both wavelengths. VGS_21 is an edge-on spiral, whose nuclear bulge is clearly seen in $3.6\mu\text{m}$ but obscured

⁴ <http://www.sdss.org/DR7/algorithms/>

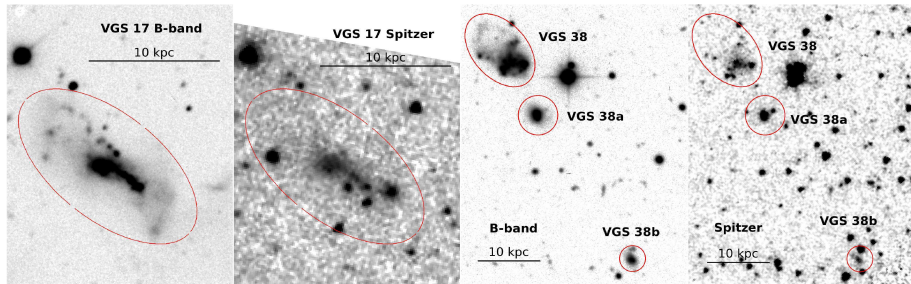
Spirals



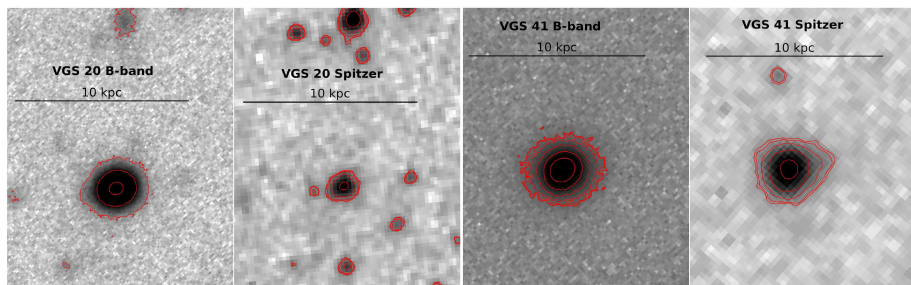
Edge-ons



Irregulars



Compact galaxies



Early-types

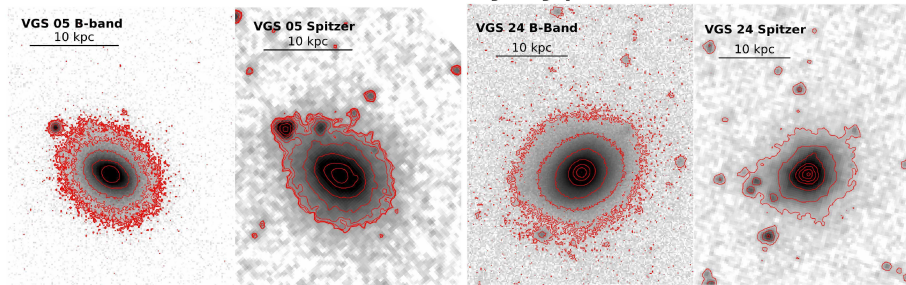


Figure 5. Examples of the different morphological representatives among the VGS void galaxies. For each morphological representation two galaxies are shown in both B and [Spitzer 3.6] band. In each image, the black bar represents a physical scale of 10 kpc. (A colour version of this figure is available in the online journal.)

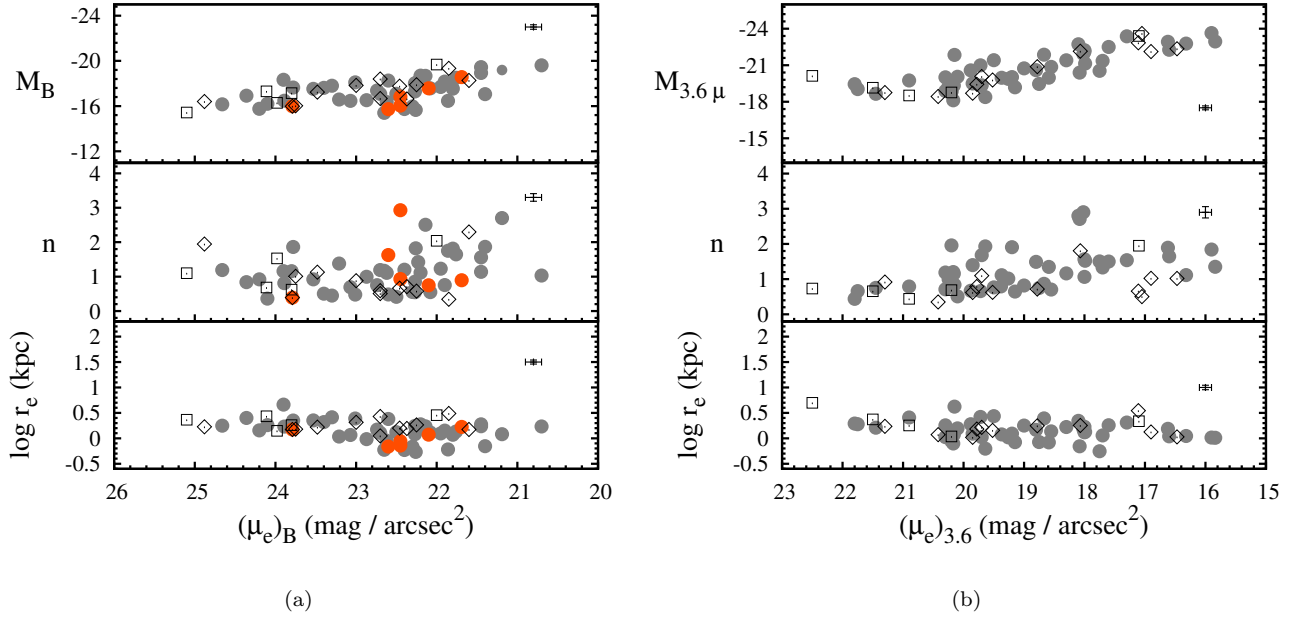


Figure 6. Absolute magnitude, Sérsic index n and the logarithm of the half-light radius r_e shown against the surface brightness at r_e (μ_e) for B-band (a) and Spitzer [3.6] band (b). The symbols are the same as in Figure 4, except that in (b) we do not distinguish galaxies depending on their seeing quality in the B-band. Typical error bars are shown in black on the righthand side of each plot. (A colour version of this figure is available in the online journal.)

by dust in B-band. VGS_50 may be an example of an edge-on S0 type galaxy. Its bulge is visible in both wavelengths, whereas its disk is only visible in the B-band. VGS_17 and VGS_38 are examples of VGS galaxies with irregular shapes. VGS_38 is a system of three galaxies embedded in the same HI envelope (Kreckel et al. 2012). In Figure 5, all three members of the system are shown. VGS_20 and VGS_41 represent what we call compact objects in our sample due to the lack of any distinguishable feature. Both of them are very blue objects without an HI detection. VGS_05 and VGS_24 are two early-type galaxies, of which VGS_24 is the only one with an identified AGN in our sample (Beygu et al. 2016). Neither of these are detected in HI.

In the following section 4.2, we find that also on the basis of their half-radii and Sérsic indices, most VGS galaxies appear to be rather small late-type disk galaxies.

4.2 Structural parameters of the VGS galaxies

Figure 6 shows the main photometric results in the B-band (Figure 6a) and in the [3.6] band (Figure 6b). Each diagram consists of three panels. From top to bottom these plots show the absolute magnitude, Sérsic index n and the half-light radius r_e as a function of the the surface brightness μ_e at radius r_e . VGS galaxies that are irregular in shape, are edge-on ($i > 70^\circ$) and/or have $\text{FWHM}_{\text{PSF}} \geq 2$ arcseconds (only for B-band) are presented with the same symbols as in Figure 4. Typical error bars are shown in black at the righthand side of each plot. Errors on the surface brightness are a combination of errors in the zero point calibration and the formal errors from the fit. Similarly, errors in the absolute magnitudes result from errors in the zero point calibration as explained in Section 3. Errors in the half-light radii er-

rors are due to the uncertainties in the sky level and they are small. The error bars are small compared to the large parameter ranges in Figure 6. And errors on the Sérsic indices are formal errors from the fit. We list the photometric results of the VGS galaxies in Table 1.

The majority of the VGS galaxies have Sérsic indices $n < 2$ in both bands and have half-light radii < 3.3 kpc, which confirms that they are small, late-type disk galaxies. A similar result is also found by Alpaslan et al. (2015) using r-band photometry. The surface brightness varies between 25 and 20 $\text{mag}/\text{arcsec}^2$ in the B-band, whereas the $3.6 \mu\text{m}$ surface brightness of the galaxies covers a wider range than in the B-band, from 23 to 15.5 $\text{mag}/\text{arcsec}^2$.

Before comparing these results to the literature data, we looked at the ratio of the $(r_e)_B$ to $(r_e)_{3.6}$ and the ratio of the n_B to $n_{3.6}$ of the VGS galaxies in order to understand the galaxy concentration properties. In Figure 7, we present the $(r_e)_B/(r_e)_{3.6}$ (top panel) and the $n_B/n_{3.6}$ ratios (lower panel) as a function of stellar mass, $(r_e)_B$ and n_B . We find that the $(r_e)_B/(r_e)_{3.6}$ increases as a function of both increasing stellar mass and increasing r_{eB} . This shows that light in the smaller galaxies is more concentrated in B than in $3.6 \mu\text{m}$. This could be caused by the fact that star formation is more concentrated in the smaller galaxies, or distributed more in the outer parts in the larger objects. Also, extinction could contribute to this relation. Larger galaxies generally contain more dust. Since this causes more extinction in the centre of the galaxy, and the extinction in the B band is more substantial, it causes the effective radius $(r_e)_B$ in the B band to be larger than the one at $(r_e)_{3.6}$. In reality, both effects probably play a role. The large scatter for the faint galaxies could be caused by the range of central star formation properties in these objects. In the absence of extinction and

young stellar populations, the r_e ratios that we observe could also be caused by metallicity gradients. Since our galaxies are spirals with both extinction and young stellar populations, this last option does not seem very likely, although it will have a small contribution.

In the lower panel of Figure 7 we see that the ratio of the Sérsic indices n_B to $n_{3.6}$ is on the order of unity. There is a slight tendency for the ratio to decrease with increasing stellar mass. It is a clear reflection of the more substantial extinction in larger galaxies, manifesting itself in a radial surface brightness profile that is less peaked in the B band. For most of the small galaxies there is no difference, suggesting a smaller effect. It also means that the star formation histories do not vary drastically as a function of radius.

To get a first broad impression of how the near-infrared $3.6 \mu\text{m}$ structural parameters of the VGS galaxies compare to those of a more average population of galaxies, we compare these to some literature samples of ellipticals and spirals. In Figure 8, we compare the VGS galaxies with a sample of galaxies that has been observed with the Spectrographic Areal Unit for Research on Optical Nebulae (SAURON) and for which structural parameters have been published by Falcón-Barroso et al. (2011). The VGS galaxies are considerably fainter than the spiral and elliptical galaxies. In this sample they are on average 2-3 magnitudes fainter. In the near-infrared regime, the VGS galaxies also have smaller Sérsic indices than ellipticals. On the other hand, VGS galaxies have near-infrared effective radii quite similar those of ellipticals and Sa galaxies.

In order to compare the structural parameters of our sample to many galaxies of different morphological types we use different structural parameters such as the central surface brightness $(\mu_0)_B$ and the scale length h in addition to the surface brightness at $(r_e)_B$, the half-light radii $(r_e)_B$, Sérsic index n and absolute magnitude M_B . Our comparison samples have not been selected on the basis of environment. Instead, they are taken from a number of papers that present carefully determined photometry of a range of galaxies.

In Figure 9a we compare our B-band photometry results with the same data used in Graham & Guzmán (2003) (Figure 9, middle panel in that paper) and in Jansen et al. (2000). The data used in Graham & Guzmán (2003) consists of a variety of dE and elliptical galaxies. There are 18 dE galaxies from the Coma Cluster selected by Graham & Guzmán (2003), a sample of 23 Virgo and Fornax Cluster dE galaxies from Stiavelli et al. (2001), another sample of dE galaxies from the Virgo Cluster studied by Binggeli & Jerjen (1998), and intermediate to bright elliptical galaxies from Caon et al. (1993) and D’Onofrio et al. (1994). The data adopted from Jansen et al. (2000) consist of spirals of type Sb to Sm. They belong to a sample of 200 nearby galaxies selected from the first CfA redshift catalogue (Davis et al. 1983). All galaxies in this sample have been morphologically classified. It includes a wide range of late type galaxies over a large range of luminosities ($M_B = -14$ to -22).

In Figure 9b, we use a sample of spiral and late-type dwarf galaxies from de Jong & van der Kruit (1994), Möllenhoff (2004) and Swaters & Balcells (2002). The spiral galaxy sample of de Jong & van der Kruit (1994) has been selected from the Uppsala General Catalogue of Galaxies (UCG) in such a way that only the S and Sb type galaxies have been included. Spiral galaxies of Möllenhoff (2004) have been se-

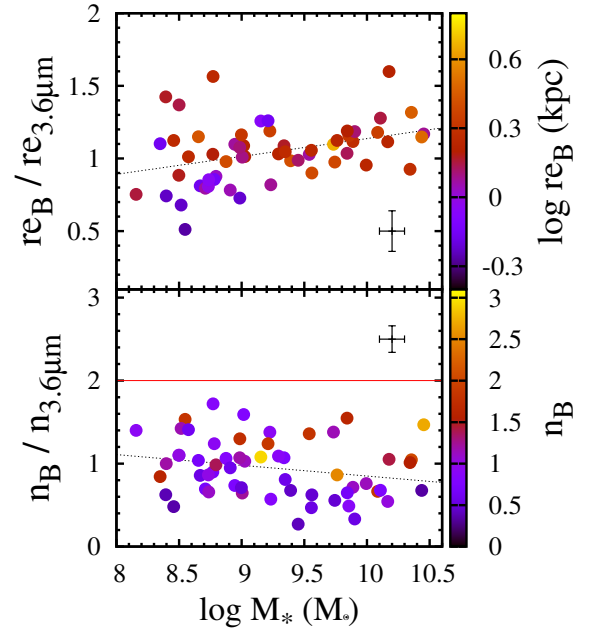


Figure 7. The ratios of the half-light radii r_e (top) and Sérsic indices n (bottom) of the B-band and $3.6\mu\text{m}$ against stellar mass M_* and colour coded as a function of $(r_e)_B$ and n_B . Typical error bars are shown in black in the corner of each plot. (A colour version of this figure is available in the online journal.)

lected from the Revised Shapley-Ames Catalogue (Sandage & Tammann 1981). These include galaxies of Hubble type from Sa to Sc without a strong bar. The late-type dwarf galaxies are a subsample of 171 late-type dwarf and irregular galaxies observed as part of the Westerbork HI Survey of Spiral and Irregular Galaxies (WHISP). Here we use 46 of them with B-band photometric data from Swaters & Balcells (2002).

VGS galaxies appear to trace the same range of surface brightness, in terms of both $(\mu_e)_B$ and $(\mu_0)_B$, as spiral galaxies and late-type dwarfs (see Figure 9a and b). Within the same range of surface brightness, the scale lengths and absolute magnitudes of the VGS galaxies are also comparable to those of late-type dwarfs in the WHISP sample and in the Jansen et al. (2000) sample. In this context, we should note that the late-type dwarfs in the WHISP sample reach out to substantially lower surface brightness levels. In comparison to more regular spiral galaxies, such as those in the spiral samples of the de Jong & van der Kruit (1994) and Möllenhoff (2004), VGS galaxies are substantially fainter and smaller. On the average, these spirals are 2.5 magnitudes brighter than the VGS galaxies.

As may be seen from Figure 9a (top panel) the VGS galaxies are fainter than ellipticals. As expected, the ellipticals have a substantially larger Sérsic index n . In fact, the indices n of ellipticals are larger than those of nearly all galaxies represented in Figure 9a (central panel). Interestingly, it turns out that the Sérsic indices as well as the effective radii of dE galaxies are of the same order as those of the VGS galaxies. Nonetheless, the VGS galaxies are substantially brighter than the dE galaxies, both in terms of absolute magnitude and effective surface brightness. The mean abso-

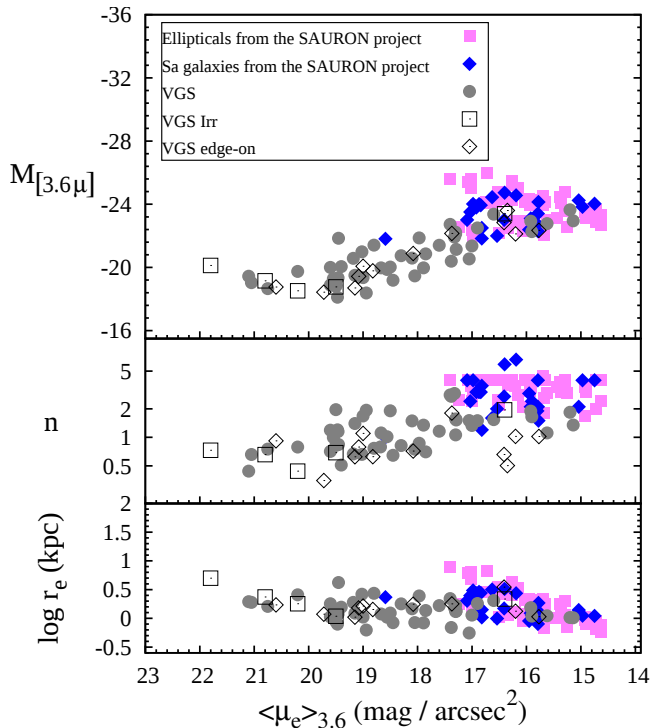


Figure 8. Absolute magnitude, Sérsic index n and the logarithm of the half-light radius r_e shown against the surface brightness at r_e (μ_e) for the Spitzer [3.6] band using a sample of galaxies that has been observed by the SAURON collaboration (Falcón-Barroso et al. 2011). Here we use the mean effective surface brightness $\langle \mu_e \rangle_{3.6}$ instead of the effective surface brightness. (A colour version of this figure is available in the online journal.)

lute magnitude of ~ -17.1 of the VGS galaxies is around ~ 1 magnitude brighter than that of the dE galaxies.

In summary, VGS galaxies have small half-light radii and scale lengths, rather similar to those of late-type dwarfs and small spirals. In terms of size and luminosity they therefore look very much like late-type dwarfs. Interestingly, their Sérsic indices are similar to dEs indicating that they have similar light distributions. However, dE’s have slightly smaller half-light radii, and a significantly smaller absolute brightness and effective surface brightness (Figure 9a).

4.3 Environment and H I content

As explained in Kreckel et al. (2011a), the void environments of the VGS galaxies are defined using a watershed delineation of the galaxy density field. The geometric and topological identification of the void regions, and the criterion that within the identified watershed basins the VGS galaxies should reside in regions with a galaxy density contrast $\delta < -0.5$ (averaged over 1 Mpc), ensures that they are located in the central interior of their voids. Within the sample, the VGS galaxies are found at an underdensity contrast δ between -0.94 to -0.52 , with an average underdensity value of $\langle \delta \rangle \approx -0.78$ when $1 h^{-1}$ Mpc Gaussian smoothing filter applied.

The void galaxy identification procedure for the VGS does not involve any criteria related to intrinsic galaxy prop-

erties like morphological type. At first glance, we would therefore not expect any dependence of the H I content and other characteristics of the VGS galaxies on the relative positions of the galaxies within their voids. However, we made some striking discoveries, in particular for several galaxies in the deepest realms of cosmic voids, i.e. with $\delta < -0.9$.

It is interesting that, of the five galaxies residing in desolate regions with $\delta < -0.9$, three are not detected in H I. Two of these are galaxies with the smallest half-light-radius of ~ 0.7 kpc in the VGS sample. They are the very compact galaxies VGS_20 and VGS_41 (Figure 5). Perhaps the most surprising finding is that of an early-type galaxy, VGS_05, which lies in the deepest underdensity of the entire sample, at $\delta \equiv -0.93$. VGS_05 is indeed a rarity amongst the void galaxies. It has a stellar mass-to-light ratio of ~ 6.8 in $3.6\mu\text{m}$, is not detected in H I, and has no detected companion, neither in the optical nor in H I. The presence of this galaxy in the sample is interesting, as it is the only example of this morphological type. Considering its high stellar mass-to-light ratio, it must have evolved much faster than the rest of the sample and consumed its H I. The remaining two galaxies at $\delta < -0.9$ are more reminiscent of other void galaxies. They are detected in H I and are blue disk galaxies with half-light radii comparable to the rest of the VGS sample.

When considering the position of void galaxies within the context of the overall structural complexity of the cosmic web, the two VGS galaxies with the most outstanding locations are VGS_31 (Beygu et al. 2013) and VGS_12 (Stanonik et al. 2009). VGS_31 is a system of three interacting system aligned along a filamentary feature in the interior of a void. It is likely that this system, discussed in detail in Beygu et al. (2013), reflects a density enhancement in an underlying tenuous dark matter filament. The other interesting case is that of VGS_12, a polar disk galaxy (for an extensive study see Stanonik et al. 2009). It is located in a tenuous wall that forms the boundary between two walls, and is amongst the most isolated objects in the nearby Universe. Even though its colour, stellar mass and star formation activity are not dissimilar from other typical void galaxies, such as VGS_20 and VGS_41, it has the uniquely interesting feature of an immense H I disk rotating perpendicular to its stellar disk. This disk may hint at the influence of its special location, which may be responsible for the cold inflow of gas from the two voids on whose boundary it is located (Stanonik et al. 2009).

In terms of structural parameters, VGS_12 has a half-light radius $(r_e)_B \approx 1.2$ kpc and a surface brightness $(\mu_e)_B \approx 23$ mag/arcsec². These are comparable to the VGS sample in general. However, it has a significantly smaller Sérsic index $n \approx 0.7$ than the mean $n = 1.1$ of the VGS sample. Two members of the VGS_31 system have a surface brightness that is higher than the mean $(\mu)_B \approx 22.7$ mag/arcsec² of the VGS sample: for VGS_31b $(\mu)_B \approx 20.7$ mag/arcsec² and VGS_31a has $(\mu)_B \approx 22$ mag/arcsec². Both are also considerably larger than the average VGS galaxy, with their half-light radii in excess of the mean, $(r_e)_B \approx 1.6$ kpc of the VGS sample.

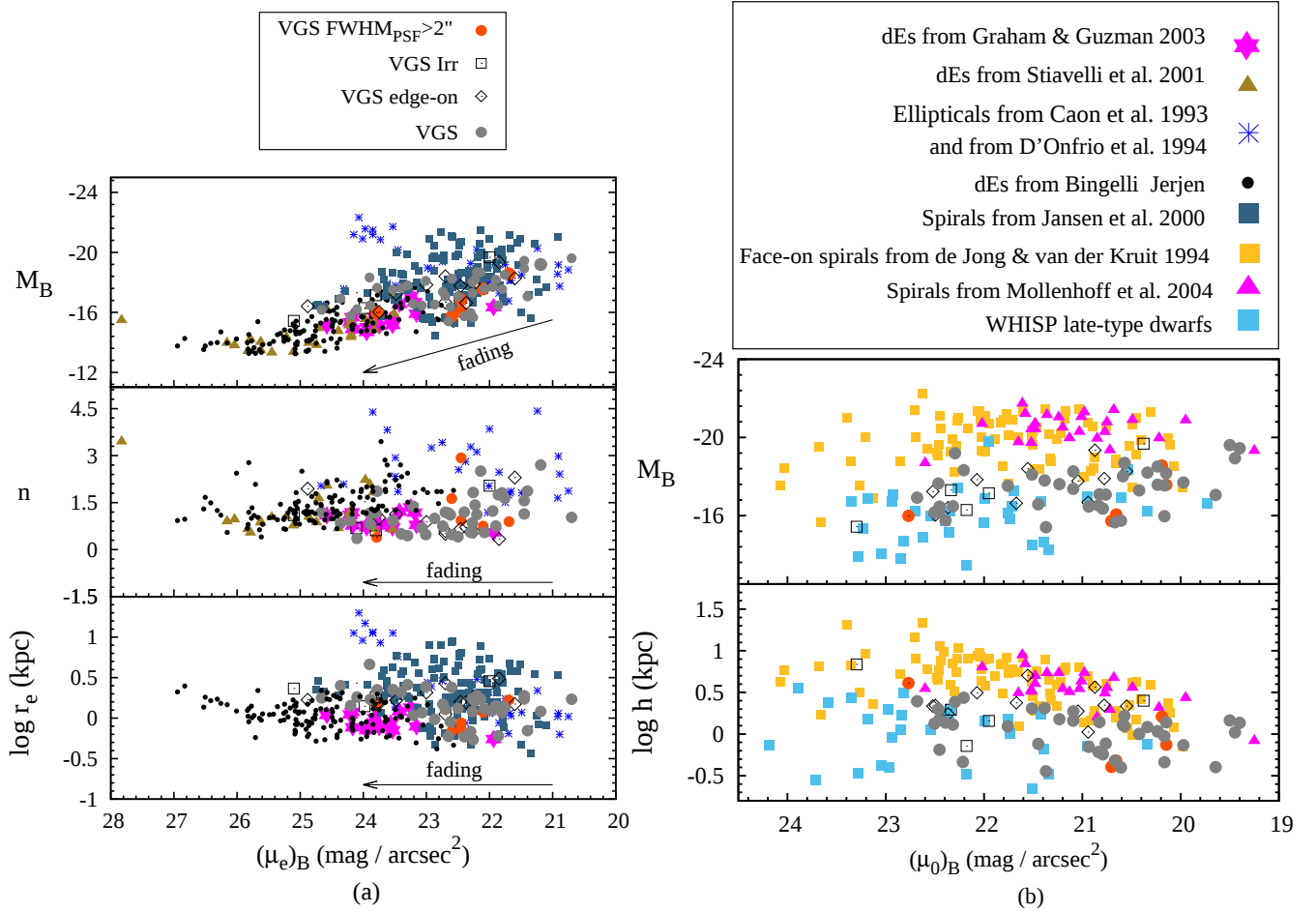


Figure 9. Comparison of the structural parameters of the VGS galaxies to the galaxies of various morphologies. a) Absolute magnitude M_B , Sérsic index n and the logarithm of the half-light radius r_e shown against the surface brightness at r_e (μ_e) for B-band. VGS galaxies are compared to the dwarf ellipticals dE and ellipticals. b) Absolute magnitude and scale length h shown against the central surface brightness (μ_0)_B where VGS galaxies are compared to spirals. In both panels, the same symbols in Figure 6a are used to represent the VGS galaxies. Pink stars represent the Coma dEs from [Graham & Guzmán \(2003\)](#), dots represent dE galaxies from [Binggeli & Jerjen \(1998\)](#), green triangles represent dE galaxies from [Stiavelli et al. \(2001\)](#), black asterisks represent intermediate to bright E galaxies from [Caon et al. \(1993\)](#) and [D’Onofrio et al. \(1994\)](#). Blue-green squares are spiral galaxies from [Jansen et al. \(2000\)](#). Yellow squares represent the face-on spiral galaxy sample from [de Jong & van der Kruit \(1994\)](#) and pink triangles are the spiral galaxy sample from [Möllenhoff \(2004\)](#). Finally light-blue squares are late-type dwarf galaxies of WHISP survey from [Swaters & Balcells \(2002\)](#). (A colour version of this figure is available in the online journal.)

5 STELLAR POPULATION EVOLUTION AND STAR FORMATION HISTORY

With the aim of assessing how the VGS galaxies have evolved, we have explored a scenario in which they remain in isolation, and gradually and uninterruptedly evolve as their current stellar population is ageing. In this scenario, galaxies will slowly become fainter and redder as their stellar populations become more and more dominated by older, fainter and redder stars. To investigate this evolutionary trend, we partially follow the work of [Meidt et al. \(2014\)](#). In this study, stellar populations presented in the 3.6 μm are purely based on stellar evolutionary tracks and observed stellar fluxes ([Benjamin et al. 2003](#); [Churchwell et al. 2009](#)). In all other stellar population models that present predictions for the 3.6 μm band ([Marigo et al. 2008](#); [Bruzual & Charlot 2003](#)), theoretical stellar atmospheres were used. However, these can

strongly over- or under-estimate the fluxes ([Peletier et al. 2012](#)).

Our calculations are based on the - strong - assumption that the stellar populations of each VGS galaxy have the same age and metallicity. Once the latter is chosen, we subsequently determine the age and stellar mass-to-light ratio in the B-band using the MILES models of [Vazdekis et al. \(2010\)](#). As a result the effects of fading, i.e. the ageing of a stellar population with time, a galaxy typically becomes fainter by ~ 2.5 magnitude over 11.58 Gyr, implying that the mass-to-light ratios will increase by these numbers. The fading process can be investigated by studying its effect in scaling relations in B-band such as presented by the arrows in Figure 9.

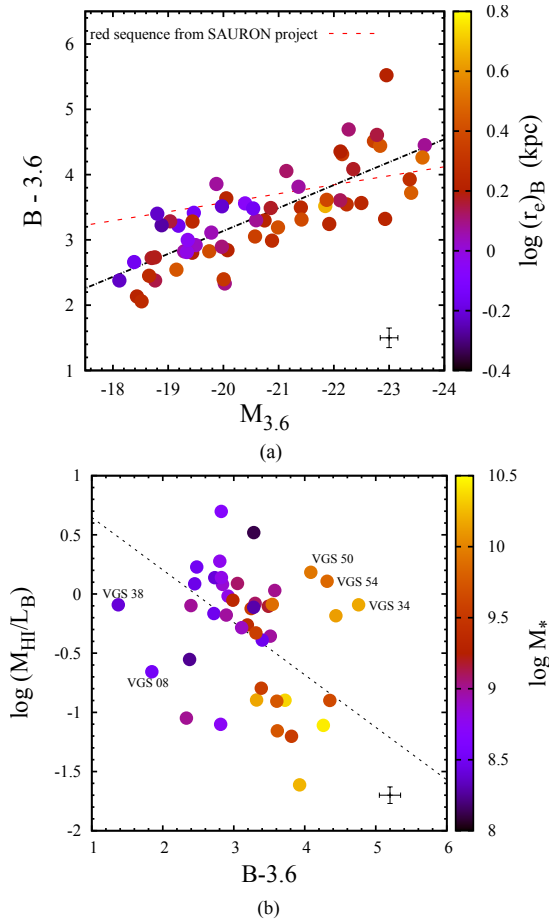


Figure 10. Relation between the $B - [3.6]$ colour, absolute magnitude $M_{3.6}$, the M_{HI} mass-to-light L_B ratio, half light radius $(r_e)_B$ and the stellar mass M_* . Top: $B - [3.6]$ colour (at half-light radii r_e) against $M_{3.6}$ and coloured with the logarithm of the $(r_e)_B$. With the red dotted line, we show the red sequence of [Falc3n-Barroso et al. \(2011\)](#). Bottom: The M_{HI} mass-to-light L_B ratio against the $B - [3.6]$ colour as a function of the stellar mass M_* . In both plots, HI non-detections are shown as upside-down triangles. Galaxies marked with their names are excluded from the linear regression due to their uncommonly high or low HI mass-to-light ratios (see text for details). (A colour version of this figure is available in the online journal.)

5.0.1 Colours, magnitudes and gas content

During their evolution, galaxies are expected to consume their gas and form fewer stars as time goes by. As a result, they turn redder and their stellar mass-to-light ratios increase. Within this scenario, we expect that the VGS galaxies that have higher HI mass-to-light ratio have lower stellar mass-to-light ratio and vice versa.

To see how viable this trend is for the VGS galaxies, we will use the results presented in Figures 10 and 11. We have added the red sequence to this diagram, following the relation inferred by [Falc3n-Barroso et al. \(2011\)](#) that concerns early-type galaxies observed with SAURON. This sequence has been defined observationally by fitting a number of non-rotating elliptical galaxies, and assuming that these galaxies consist purely of old stars.

The first observation from top panel of Figure 10a is that the redder, and brighter, VGS galaxies have larger ef-

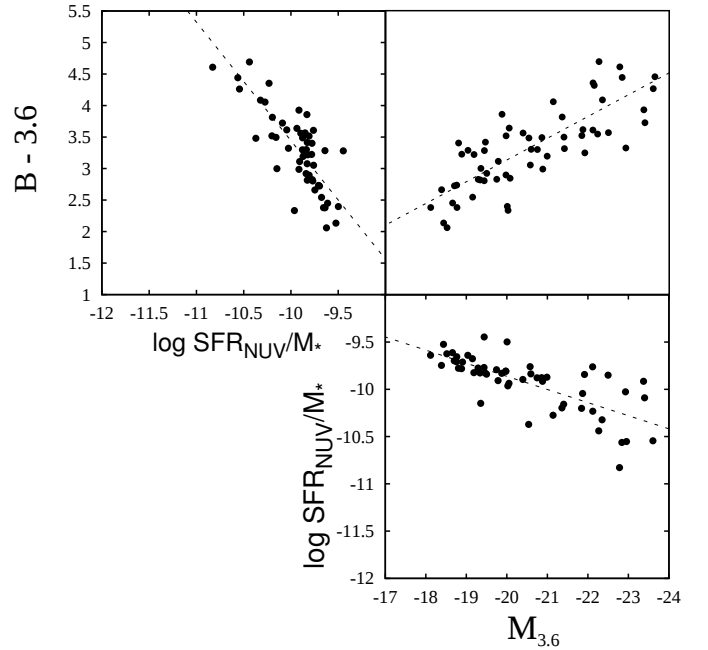


Figure 11. Relations between the $B - [3.6]$ colour, specific star formation rate in the near-UV ($\text{SFR}_{\text{NUV}}/M_*$) and the magnitude $M_{3.6}$ are presented in three panels.

fective radii. The vertical distance to the red sequence indicates the blueing by young stellar populations. This is a measure of the galaxy age, independent of metallicity. We see that most of the massive VGS galaxies fall above the red sequence, indicating that these objects are reddened by dust. It also means that the $B - [3.6]$ colour cannot give much information about the stellar population of the galaxies. The smaller galaxies all lie below the red sequence. The distance to the red sequence increases with decreasing magnitude for the most massive galaxies. This indicates that the faintest galaxies are probably the youngest, and are beset by the lowest extinction. The bottom panel of Figure 10 shows the relation between HI mass-to-light ratio and $B - [3.6]$ colour as a function of stellar mass from the $3.6\mu\text{m}$ photometry. The linear regression does not include the HI non-detections (marked by upside-down triangles), nor the galaxies marked with their names. As expected, and in accordance with [Kreckel et al. \(2012\)](#), the M_{HI} -to- L_B ratio is a decreasing function of stellar mass. There are a few galaxies with uncommonly high or low M_{HI} -to- L_B ratios for their stellar mass and colour. In the diagrams, these are indicated by their names. VGS_34, 50 and 54 are still M_{HI} -rich, given the fact that they are red and do not actively form stars (upper left panel of Figure 11). On the other hand, VGS_08 and VGS_38 have much lower M_{HI} -to- L_B ratios than should be expected, given the fact that they are quite blue and are star-forming galaxies (Figure 11). These galaxies have an irregular shape and the HI disk of VGS_38 shows in particular strong signs of interaction and therefore has large uncertainties in the estimate of the total HI mass. This is also true for VGS_25 and VGS_31b.

5.0.2 Star formation activity and history

Figure 11 shows the relations between the $B - [3.6]$ colour, specific star formation rate in the near-UV ($\text{SFR}_{\text{NUV}}/M_*$) and the absolute magnitude $M_{3.6}$. From top to bottom, we first present the $B - [3.6]$ colour as a function of the $\text{SFR}_{\text{NUV}}/M_*$ and as a function of the $M_{3.6}$, then the $\text{SFR}_{\text{NUV}}/M_*$ as a function of the $M_{3.6}$. VGS_05 is excluded from the plots.

The Near-UV star formation rates (SFR_{NUV}) have been calculated from the Galaxy Evolution Explore (GALEX) near-UV luminosities, corrected for internal dust attenuation following the method outlined in Schiminovich et al. (2010).

$$\text{SFR}_{\text{UV}} [M_{\odot} \text{yr}^{-1}] = \frac{L_{\text{UV}} f_{\text{UV}}(\text{young}) 10^{0.4A_{\text{UV}}}}{\eta_{\text{UV}}}, \quad (8)$$

where L_{UV} is the luminosity in $\text{erg s}^{-1} \text{Hz}^{-1}$, $f_{\text{UV}}(\text{young})$ is the fraction of light that originates in young stellar populations, η_{UV} is the conversion factor between UV luminosity and recent-past-averaged star formation rate and A_{UV} is the dust attenuation. Following Schiminovich et al. (2010), we assume $f_{\text{UV}}(\text{young}) = 1$ and $\eta_{\text{UV}} = 10^{28.165}$. (see Beygu et al. 2016, for details).

We find, not unexpectedly, that the $B - [3.6]$ colour is an increasing function of the specific star formation measured in the near-UV:

$$B - [3.6] = -1.88 \times \text{SFR}_{\text{NUV}}/M_* - 15.37, \quad (9)$$

(top-left panel Figure 11) and of the absolute magnitude $M_{3.6}$,

$$B - [3.6] = -0.34 \times M_{3.6} - 3.76, \quad (10)$$

(top-right panel Figure 11).

The specific star formation is a linear function of the absolute magnitude $M_{3.6}$ as well. However, the slope of 0.14 is much smaller than the gradient of the ($B - [3.6]$) versus $\text{SFR}_{\text{NUV}}/M_*$ relation and the ($B - [3.6]$) versus $M_{3.6}$ relation. The logarithm of the $\text{SFR}_{\text{NUV}}/M_*$ changes only ~ 1 dex over a ~ 5.5 magnitude range in absolute magnitude $M_{3.6}$. This suggests that both the near-UV and $B - [3.6]$ are probing the star formation properties of the VGS galaxies. More detailed modelling is needed to find out how these two observables can be combined. This is not straightforward, given the effects of extinction.

6 DISCUSSION

Given the often isolated environment, we may expect that the majority of void galaxies evolve secularly. The effect of the void environment is mainly that of limiting the mass of the galaxies that emerge in their interior. This is simply because of the absence of a sufficient amount of matter: the galaxy (halo) mass function is significantly shifted to lower masses (see e.g. Aragón-Calvo et al. 2010a; Cautun et al. 2014, for a systematic appraisal of this effect). However, this raises the question of why the equivalent low-mass galaxies in higher density regions are not more seriously affected by environmental physical processes. The answer may lie in the past. At the time of their formation, void environments also involved a considerably higher density environment than we

see at present. This can indeed be seen in computer simulations of structure formation (see e.g. Springel et al. 2005; Vogelsberger et al. 2014).

This should lead us to investigate in more detail the possibly direct environmental impact on void galaxies, which in most situations will have been restricted to earlier cosmic epochs. However, in some situations there may be a hint of more direct environmental impact on a galaxy’s life, or of a less straightforward evolutionary path, in the population of void galaxies that we have observed in the VGS survey.

At this point the VGS and some of the recent studies draw our attention to the following findings. First, void galaxies with stellar masses $\leq 10^{10} M_{\odot}$ are blue late type star forming galaxies. Their star formation properties are not significantly different from the galaxies that reside in fields, or moderate density environments (Alpaslan et al. 2015; Penny et al. 2015; Beygu et al. 2016) suggesting that stellar mass is the dominant factor which regulates the galaxy properties. They are gas rich galaxies with diverse HI properties, from regular rotation to disturbed gas morphologies and kinematics (Kreckel et al. 2011a, 2012). The HI irregularities are evidence of ongoing interactions and gas accretion while regular rotating disks suggest secular evolution (see Kreckel et al. 2012, for details).

Second, if the effect of the void environment is mainly that of limiting the mass of the void galaxies, than is there an upper limit on the stellar mass? The void galaxy sample of the VGS doesn’t include any galaxy with stellar mass $> 3 \times 10^{10} M_{\odot}$ suggesting that the void environment has an effect on the size of galaxies, whereas the void galaxy sample of Alpaslan et al. (2015) and Penny et al. (2015) have massive galaxies with stellar mass up to $5 \times 10^{11} M_{\odot}$. Moreover, these massive void galaxies regardless of their star formation activity seem to be disk galaxies. Based on their colour and morphology Penny et al. (2015) argue that these massive void galaxies could have extinguished their gas supply, and have not undergone the interactions and mergers required to transform them into elliptical galaxies due to their isolation. On the other hand one of the three galaxies (VGS_05) in the VGS with stellar mass of the order of $10^{10} M_{\odot}$, is an elliptical galaxy with no star formation activity detected either in optical or near-infrared and not detected in HI. The other two VGS galaxies are star forming spirals.

This raises the question how do void galaxies acquire their mass and can voids harbour galaxies as massive as those found in dense environments? Massive ellipticals are believed to accumulate mass via interactions and major mergers whereas disk galaxies via star formation and accretion of small satellites (Schweizer 2000; Kauffmann et al. 2003, 2004; van Dokkum 2005). Given its stellar mass of $2 \times 10^{10} M_{\odot}$, VGS_05 is not a typical massive elliptical galaxy but an early-type galaxy that reside very close to the centre of its parent void ($\delta \equiv -0.93$). Is VGS_05 an example of secular evolution or was it subject to interactions and major mergers very early in time compared to the rest of 58 void galaxies in the VGS sample? The same is true for the second early-type galaxy in the VGS, VGS_24, that is an AGN.

On the other hand the existence of pairs and group of galaxies living in voids which show strong signs of interactions presents evidence for non secular galaxy evolution. Two such examples are VGS_31 and VGS_38. VGS_31 is a group of three interacting galaxies embedded in the same

HI envelope (see [Beygu et al. 2013](#), for details). The group also shows sign for minor merger and triggered star formation activity. We explored the dynamical and environmental origin and development of VGS_31 in some detail ([Rieder et al. 2013](#)). Our study revealed the often surprisingly complex and diverse dynamical evolution of the intravoids cosmic web of tenuous — usually underdense — filamentary and sheetlike structures. Quite reminiscent of the possibility of such an imprint of large-scale evolution on the nature of a void galaxy is the case of the polar ring galaxy VGS_12 ([Stanonik et al. 2009](#)). VGS_38 in a group of three galaxies has clearly undergone major merger as seen in the HI velocity map ([Kreckel et al. 2011a, 2012](#)) and optical morphology (Figure 5), is another example for rare major merger events in voids.

Galaxies grow via the inflow and infall of gas from the environment. From numerous simulation studies, we are beginning to understand that the morphology of galaxies may be determined to a considerable extent by the nature of the web-like structures in which they are embedded. The gas is channelled out of voids and transported via gaseous tendrils into the emerging galaxies (e.g. [Dekel et al. 2009](#); [Hahn et al. 2010](#); [Pichon et al. 2011](#); [Codis et al. 2012](#); [Rieder et al. 2013](#); [Aragón-Calvo & Szalay 2013](#); [Aragón-Calvo et al. 2016](#), and references therein). The void galaxies in the VGS survey, located in a well-defined large-scale environment, will provide us with crucial information on how their structure and morphology, as well as their star formation activity, may indeed be dependent on not only mass but also on the environmental dynamics indicated by the most recent cosmological simulations.

7 CONCLUSION

We analysed Spitzer 3.6 and 4.5 μ m and B-band imaging of 59 void galaxies as part of the Void Galaxy Survey (VGS) to study their colour, stellar mass, galaxy concentration, morphology and star formation properties. The main conclusions are:

- We find that our void galaxy sample mostly consists of late-type galaxies. Most of them are similar to (Sd-Sm) galaxies, although a few are earlier type spirals and some are irregularly shaped galaxies.
- The VGS galaxies have small half-light radii and scale lengths, rather similar to those of late-type dwarfs and small spirals. In terms of size, morphology and colour properties they clearly resemble late-type galaxies.
- Interestingly, the light distributions of VGS galaxies bear some resemblance to that of dE galaxies. Like the latter, in both wavelength regimes their Sérsic indices are smaller than 2, $n < 2$.
- They span a wide colour range in $B - [3.6]$ and most of them are blue, gas rich and star forming galaxies. An occasional VGS galaxy is gas poor, small and blue. However, they cover a considerable range of morphological types and different star formation properties ([Beygu et al. 2016](#)). The same is true for their hydrogen gas content ([Kreckel et al. 2012](#)).
- The voids in our sample do not appear to be populated by a particular type of void galaxy and despite the very low-surface-brightness limit of our B-band images, we have not

found any dwarfs or small galaxies with $M_* < 10^7 M_\odot$. After deriving the stellar masses using near-infrared images, we confirmed the upper limit of $10^{10.5} M_\odot$ inferred by [Kreckel et al. \(2012\)](#). We can conclude that the most prominent effect of the void environments is that it prohibits the formation of large and massive galaxies.

ACKNOWLEDGEMENTS

The authors wish to thank the anonymous referee, for a careful assessment of the manuscript and very useful comments. We would like to thank M. Querejeta and S. Meidt for sharing their S4G nearby galaxy stellar mass catalogue. This work was supported in part by the National Science Foundation under grant no. 1009476 to Columbia University. We are grateful for support from J. H. van Gorkom's Da Vinci Professorship at the Kapteyn Astronomical Institute. J.M. van der Hulst acknowledges support from the European Research Council under the European Union's Seventh Framework Programme (FP/2007-2013)/ ERC Grant Agreement nr. 291531. K. Kreckel acknowledges grant KR 4598/1-2 from the DFG Priority Program 1573. The Isaac Newton Telescope is operated on the island of La Palma by the Isaac Newton Group in the Spanish Observatorio del Roque de los Muchachos of the Instituto de Astrofísica de Canarias. This work is based on observations made with the Spitzer Space Telescope, which is operated by the Jet Propulsion Laboratory, California Institute of Technology under a contract with NASA. Support for this work was provided by NASA.

REFERENCES

- Alpaslan M., et al., 2014, *MNRAS*, **440**, L106
 Alpaslan M., et al., 2015, *MNRAS*, **451**, 3249
 Aragón-Calvo M. A., 2012, preprint, ([arXiv:1210.7871](#))
 Aragón-Calvo M. A., Szalay A. S., 2013, *MNRAS*, **428**, 3409
 Aragón-Calvo M. A., van de Weygaert R., Jones B. J. T., 2010a, *MNRAS*, **408**, 2163
 Aragón-Calvo M. A., Platen E., van de Weygaert R., Szalay A. S., 2010b, *ApJ*, **723**, 364
 Aragón-Calvo M. A., Neyrinck M. C., Silk J., 2016, preprint, ([arXiv:1607.07881](#))
 Benjamin R. A., et al., 2003, *PASP*, **115**, 953
 Beygu B., Kreckel K., van de Weygaert R., van der Hulst J. M., van Gorkom J. H., 2013, *AJ*, **145**, 120
 Beygu B., Kreckel K., van der Hulst J. M., Jarrett T. H., Peletier R., van de Weygaert R., van Gorkom J. H., Aragón-Calvo M. A., 2016, *MNRAS*, **458**, 394
 Bingeli B., Jerjen H., 1998, *A&A*, **333**, 17
 Bruzual G., Charlot S., 2003, *MNRAS*, **344**, 1000
 Buta R. J., 2013, *Galaxy Morphology*. p. 155
 Caon N., Capaccioli M., D'Onofrio M., 1993, *MNRAS*, **265**, 1013
 Cautun M., van de Weygaert R., Jones B. J. T., Frenk C. S., 2014, *MNRAS*, **441**, 2923
 Ceccarelli L., Padilla N. D., Valotto C., Lambas D. G., 2006, *MNRAS*, **373**, 1440
 Churchwell E., et al., 2009, *PASP*, **121**, 213
 Codis S., Pichon C., Devriendt J., Slyz A., Pogosyan D., Dubois Y., Sousbie T., 2012, *MNRAS*, **427**, 3320
 Croton D. J., et al., 2005, *MNRAS*, **356**, 1155
 Cruzen S., Wehr T., Weistrop D., Angione R. J., Hoopes C., 2002, *AJ*, **123**, 142

Table 1. Col.(1): Galaxy name. Col.(2): SDSS Petrosian half-radius in SDSS r-band. Col.(3): SDSS Petrosian half-radius in SDSS g-band. Col.(4): B-band Sérsic index. Col.(5): Effective radius in B-band. Col.(6): Effective surface brightness in B-band. Col.(7): [3.6] Sérsic index. Col.(8): Effective radius in [3.6]. Col.(9): Effective surface brightness in [3.6]. Col.(10): Absolute magnitude in B-band. Col.(11): Absolute magnitude in [3.6]. Col.(12): $B - [3.6]$ colour. Col.(13): Seeing. (The full table is available online).

Galaxy	$(r_{P50})_r$	$(r_{P50})_g$	n_B	$(r_e)_B$	$(\mu_e)_B$	$n_{3.6}$	$(r_e)_{3.6}$	$(\mu_e)_{3.6}$	M_B	$M_{3.6}$	$(B - 3.6)$	$FWHM_{PSF}$
(1)	(kpc)	(kpc)	(4)	(kpc)	(mag/arcsec ²)	(7)	(kpc)	(mag/arcsec ²)	(mag)	(mag)	(12)	(arcsec)
(1)	(2)	(3)	(4)	(5)	(6)	(7)	(8)	(9)	(10)	(11)	(12)	(13)
VGS_01	0.88	0.8	0.75	1.18	22.29	1.02	1.05	19.47	-19.87	-17.57	2.3	3
VGS_02	1.63	1.73	0.81	1.8	23.96	0.51	1.57	20.35	-20.05	-16.48	3.58	1
VGS_03	0.76	0.76	0.55	0.87	22.21	0.65	0.83	19.15	-19.19	-15.97	3.22	1.3
VGS_04	0.55	0.53	2.93	0.87	21.13	2.71	0.7	17.58	-20.39	-16.83	3.56	2.3
VGS_05	2.1	2.17	1.86	2.9	23.42	2.8	2.2	18.57	-22.73	-17.64	5.08	1.6

D’Onofrio M., Capaccioli M., Caon N., 1994, *MNRAS*, **271**, 523
 Davis M., Huchra J., Latham D., 1983, in Abell G. O., Chincarini G., eds, *IAU Symposium Vol. 104, Early Evolution of the Universe and its Present Structure*. pp 167–172
 Dekel A., et al., 2009, *Nature*, **457**, 451
 Dressler A., 1980, *ApJ*, **236**, 351
 Dressler A., Thompson I. B., Shectman S. A., 1985, *ApJ*, **288**, 481
 Driver S. P., et al., 2011, *MNRAS*, **413**, 971
 Falcón-Barroso J., et al., 2011, *MNRAS*, **417**, 1787
 Franx M., Illingworth G., Heckman T., 1989, *AJ*, **98**, 538
 Freeman K. C., 1970, *ApJ*, **160**, 811
 Fukugita M., Ichikawa T., Gunn J. E., Doi M., Shimasaku K., Schneider D. P., 1996, *AJ*, **111**, 1748
 Gabor J. M., Davé R., Finlator K., Oppenheimer B. D., 2010, *MNRAS*, **407**, 749
 Goldberg D. M., Jones T. D., Hoyle F., Rojas R. R., Vogeley M. S., Blanton M. R., 2005, *ApJ*, **621**, 643
 Graham A. W., Driver S. P., 2005, *Publ. Astron. Soc. Australia*, **22**, 118
 Graham A. W., Guzmán R., 2003, *AJ*, **125**, 2936
 Grogin N. A., Geller M. J., 1999, *AJ*, **118**, 2561
 Grogin N. A., Geller M. J., 2000, *AJ*, **119**, 32
 Gunn J. E., Gott III J. R., 1972, *ApJ*, **176**, 1
 Hahn O., Teyssier R., Carollo C. M., 2010, *MNRAS*, **405**, 274
 Hoyle F., Vogeley M. S., 2002, *ApJ*, **566**, 641
 Hoyle F., Rojas R. R., Vogeley M. S., Brinkmann J., 2005, *ApJ*, **620**, 618
 Hoyle F., Vogeley M. S., Pan D., 2012, *MNRAS*, **426**, 3041
 Jansen R. A., Franx M., Fabricant D., Caldwell N., 2000, *ApJS*, **126**, 271
 Karachentsev I. D., Kaisina E. I., 2013, preprint, ([arXiv:1305.4791](https://arxiv.org/abs/1305.4791))
 Karachentseva V. E., Karachentsev I. D., Richter G. M., 1999, *A&AS*, **135**, 221
 Kauffmann G., et al., 2003, *MNRAS*, **341**, 33
 Kauffmann G., White S. D. M., Heckman T. M., Ménard B., Brinchmann J., Charlot S., Tremonti C., Brinkmann J., 2004, *MNRAS*, **353**, 713
 Kent S. M., 1985, *ApJS*, **59**, 115
 Koopmann R. A., Kenney J. D. P., 2004, *ApJ*, **613**, 851
 Kreckel K., et al., 2011a, *AJ*, **141**, 4
 Kreckel K., Peebles P. J. E., van Gorkom J. H., van de Weygaert R., van der Hulst J. M., 2011b, *AJ*, **141**, 204
 Kreckel K., Platen E., Aragón-Calvo M. A., van Gorkom J. H., van de Weygaert R., van der Hulst J. M., Beygu B., 2012, *AJ*, **144**, 16
 Kreckel K., Croxall K., Groves B., van de Weygaert R., Pogge R. W., 2015, *ApJ*, **798**, L15
 Kuhn B., Hopp U., Elsaesser H., 1997, *A&A*, **318**, 405
 Larson R. B., Tinsley B. M., Caldwell C. N., 1980, *ApJ*, **237**, 692
 Marigo P., Girardi L., Bressan A., Groenewegen M. A. T., Silva L., Granato G. L., 2008, *A&A*, **482**, 883
 Meidt S., et al., 2014, in *American Astronomical Society Meeting Abstracts*. p. 453.16
 Möllenhoff C., 2004, *A&A*, **415**, 63
 Moore B., Katz N., Lake G., Dressler A., Oemler A., 1996, *Nature*, **379**, 613
 Moorman C. M., Vogeley M. S., Hoyle F., Pan D. C., Haynes M. P., Giovanelli R., 2014, *MNRAS*, **444**, 3559
 Moorman C. M., Vogeley M. S., Hoyle F., Pan D. C., Haynes M. P., Giovanelli R., 2015, *ApJ*, **810**, 108
 Oemler Jr. A., 1974, *ApJ*, **194**, 1
 Patiri S. G., Betancort-Rijo J. E., Prada F., Klypin A., Gottlöber S., 2006a, *MNRAS*, **369**, 335
 Patiri S. G., Prada F., Holtzman J., Klypin A., Betancort-Rijo J., 2006b, *MNRAS*, **372**, 1710
 Peebles P. J. E., 2001, *ApJ*, **557**, 495
 Peletier R. F., Davies R. L., Illingworth G. D., Davis L. E., Cawson M., 1990, *AJ*, **100**, 1091
 Peletier R. F., et al., 2012, *MNRAS*, **419**, 2031
 Peng Y.-j., et al., 2010, *ApJ*, **721**, 193
 Penny S. J., et al., 2015, *MNRAS*, **453**, 3519
 Petrosian V., 1976, *ApJ*, **209**, L1
 Petrov G., Kniazev A. Y., Fried J. W., 2005, *Aerospace Research in Bulgaria*, **20**, 120
 Pichon C., Pogosyan D., Kimm T., Slyz A., Devriendt J., Dubois Y., 2011, *MNRAS*, **418**, 2493
 Platen E., van de Weygaert R., Jones B. J. T., 2007, *MNRAS*, **380**, 551
 Popescu C. C., Hopp U., Elsaesser H., 1997, *A&A*, **325**, 881
 Pustilnik S. A., Tepliakova A. L., Kniazev A. Y., 2011, *Astrophysical Bulletin*, **66**, 255
 Pustilnik S. A., Martin J.-M., Lyamina Y. A., Kniazev A. Y., 2013, *MNRAS*, **432**, 2224
 Rieder S., van de Weygaert R., Cautun M., Beygu B., Portegies Zwart S., 2013, *MNRAS*, **435**, 222
 Rojas R. R., Vogeley M. S., Hoyle F., Brinkmann J., 2004, *ApJ*, **617**, 50
 Rojas R. R., Vogeley M. S., Hoyle F., Brinkmann J., 2005, *ApJ*, **624**, 571
 Sandage A., Tammann G. A., 1981, *A revised Shapley-Ames Catalog of bright galaxies*
 Schaap W. E., van de Weygaert R., 2000, *A&A*, **363**, L29
 Schiminovich D., et al., 2010, *MNRAS*, **408**, 919
 Schlegel D. J., Finkbeiner D. P., Davis M., 1998, *ApJ*, **500**, 525
 Schombert J., 2007, *ArXiv Astrophysics e-prints*,
 Schweizer F., 2000, in *Astronomy, physics and chemistry of H⁺₃*. p. 2063 ([arXiv:astro-ph/0002263](https://arxiv.org/abs/astro-ph/0002263)), doi:10.1098/rsta.2000.0630
 Sheth R. K., van de Weygaert R., 2004, *MNRAS*, **350**, 517
 Springel V., et al., 2005, *Nature*, **435**, 629

- Stanonik K., Platen E., Aragón-Calvo M. A., van Gorkom J. H., van de Weygaert R., van der Hulst J. M., Peebles P. J. E., 2009, *ApJ*, **696**, L6
- Stiavelli M., Miller B. W., Ferguson H. C., Mack J., Whitmore B. C., Lotz J. M., 2001, *AJ*, **121**, 1385
- Swaters R. A., Balcells M., 2002, *A&A*, **390**, 863
- Szomoru A., van Gorkom J. H., Gregg M. D., Strauss M. A., 1996, *AJ*, **111**, 2150
- Tavasoli S., Rahmani H., Khosroshahi H. G., Vasei K., Lehnert M. D., 2015, *ApJ*, **803**, L13
- Tikhonov A. V., Karachentsev I. D., 2006, *ApJ*, 653, 969
- Vazdekis A., Sánchez-Blázquez P., Falcón-Barroso J., Cenarro A. J., Beasley M. A., Cardiel N., Gorgas J., Peletier R. F., 2010, *MNRAS*, **404**, 1639
- Vogelsberger M., et al., 2014, *Nature*, **509**, 177
- Wegner G., Grogin N. A., 2008, *AJ*, 136, 1
- Wetzel A. R., Tinker J. L., Conroy C., 2012, *MNRAS*, **424**, 232
- de Jong R. S., van der Kruit P. C., 1994, *A&AS*, **106**, 451
- van Dokkum P. G., 2005, *AJ*, **130**, 2647
- van de Weygaert R., Platen E., 2011, *International Journal of Modern Physics Conference Series*, **1**, 41
- van de Weygaert R., van Kampen E., 1993, *MNRAS*, 263, 481
- van de Weygaert R., et al., 2011, *The Void Galaxy Survey*. p. 17, doi:10.1007/978-3-642-20285-8_3

This paper has been typeset from a $\text{\TeX}/\text{\LaTeX}$ file prepared by the author.